POLISH MARITIME RESEARCH 2 (118) 2023 Vol. 30; pp. 130-145
10.2478/pomr-2023-0029

EVALUATION OF GEOMETRICAL INFLUENCE ON THE HYDRODYNAMIC CHARACTERISTICS AND POWER ABSORPTION OF VERTICAL AXISYMMETRIC WAVE ENERGY CONVERTERS IN IRREGULAR WAVES

Wanchao Zhang*
College of Naval Architecture and Ocean Engineering, Jiangsu University of Science and Technology, Zhenjiang, China
Yang Zhu
Jiangsu University of Science and Technology, China
Shuxu Liu
Jiangsu University of Science and Technology, China
Jianhua Wang
The PLA Troops 92228, China
Wentian Zhang
The PLA Troops 92228, China

* Corresponding author: *zhangwanchao@just.edu.cn (Wanchao Zhang)*

ABSTRACT

To obtain the mechanical energy of waves from arbitrary directions, the vibration absorbers of wave energy converters (WEC) are usually vertically axisymmetric. In such case, the wave-body interaction hydrodynamics is an essential research topic to obtain high-efficiency wave energy. In this paper, a semi-analytical method of decomposing the complex axisymmetric boundary into several ring-shaped stepped surfaces based upon the boundary approximation method (BAM) is introduced and examined. The hydrodynamic loads and parameters, such as the wave excitation forces, added mass and radiation damping of the vertical axisymmetric oscillating buoys, can then be achieved by using the new boundary discretisation method. The calculations of the wave forces and hydrodynamic coefficients show good convergence with the number of discretisation increases. Comparison between the constringent results and the results of the conventional method also verifies the feasibility of the method. Then, simulations and comparisons of the hydrodynamic forces, motions and wave power conversions of the buoys with series draught and displacement ratios in regular and irregular waves are conducted. The calculation results show that the geometrical shape has a great effect on the hydrodynamic and wave power conversion performance of the absorber. In regular waves, though the concave buoy has the lowest wave conversion efficiency, it has the largest frequency bandwidth for a given draught ratio, while in irregular waves, for a given draught ratio, the truncated cylindrical buoy has the best wave power conversion, and for a given displacement of the buoy, the concave buoy shows the best wave power conversion ability.

Keywords: Vertical axisymmetric, Ring-shaped stepped surface, Boundary approximation, Constringent, Geometrical shape

INTRODUCTION

Slow-speed ocean waves have now been proved to be a promising renewable resource that can promote the periodic vibration of the floating structure or the periodic compression and release of air, thus converting energy [1]. For this reason, and based on this principle, many wave energy converter (WEC) concepts have been developed for efficient and economic power absorption, such as the point absorber (PA), which utilises the heave mode of the oscillating buoy in waves. At the same time, the wave–body interaction hydrodynamics, as well as the performance analysis of the power take-off (PTO) mechanism, have also been continuously studied to facilitate the design of equipment and achieve the best operation in the considered environment.

The influence of the geometry influence on hydrodynamic characteristics has been evaluated on traditional marine structures to minimise their motion and improve their sea-keeping ability [2]-[3]. In contrast, the same efforts have been made in the case of PAWECs in order to make the absorber oscillate harmoniously in random sea waves, allowing maximum motion amplitudes to absorb more wave power. Many works on improving the wave power conversion efficiency by optimising the geometrical shape or parameters of PAWECs have been conducted in view of the increasing interest in ocean renewable energy [4]-[6]. Mavrakos and Katsaounis [7] explored the effect of the floaters' geometries on the power conversion performance of tightly moored vertical axisymmetric wave energy converters. The absorbers, considering a bottom-mounted vertical or horizontal skirt in the single-body and piston-like arranged WECs, were examined and comparatively assessed. They found that the conical absorber with a vertical skirt, considering the same displacement, has a better power conversion ability as the significant wave height increases. A surge–pitch wave energy converter with bi-cubic B-spline surfaces of parametric description was examined by McCabe et al. [8]. The elementary cost function was used to determine the performance, and the optimal shape of the collector was obtained by using genetic algorithms. They found that the optimal collector shape with the best cost function value overall was asymmetrical, with a bulbous body and 'wings' that slope backwards from the bottom upwards. Similar research on shape optimisation using a genetic algorithm was also conducted later by McCabe [9], considering the constraint regimes defined by the displacement and power rating limits based on wave data from the North-East Atlantic Ocean. Zhang et al. [10] introduced a new hydrodynamic evaluation method for vertical axisymmetric absorbers and explored several cases for the optimisation of wave energy conversion. They found that, among absorbers with the same outer radius and draught, the cylindrical type shows an excellent wave energy conversion ability at certain given frequencies, while in random sea waves, the parabolic and conical ones have better stabilisation and applicability in wave power conversion. Shadman et al. [11] presented a methodology for the geometrical optimisation of wave energy converters based on statistical analysis methods and the hydrodynamics of the system in the frequency domain. They tested this method on an axisymmetric heaving point absorber for a nearshore region of the Rio de Janeiro coast and obtained the optimal geometrical configuration. Esmaeilzadeh and Alam [12] calculated the optimum shape for a submerged planar pressure differential wave energy converter through a systematic method based on high-performance computing and considering different kinds of incident waves. A new parametric description of the absorber shape with Fourier decomposition of geometrical shapes is introduced in their research. Very recently, Erselcan and Kükner [13] conducted a parametric optimisation study to find an optimal design for a heaving point absorber wave energy converter located off the Turkish coast of the Black Sea. The effects of the geometry, mass, and the dimensions of the floats and the parameters of the power take-off system are considered and evaluated.

The above series of optimisation studies are based upon the accurate simulation of the hydrodynamics of wave power harvesting structures. For those oscillating absorbers with a simple configuration, the traditional potential flow algorithm, dividing the encircled fluid domain into several subdomains, can be employed. In such case, the expressions of the velocity potentials, added mass, radiation damping and wave forcing can be analytically presented by using the eigenfunction expansion method as shown in Mavrakos et al. [14] and Bachynski et al. [15]. Thus, the hydrodynamic performance as affected by the geometrical parameters can be systematically described. However, for absorbers with a complex wetted surface, numerical calculation methods (boundary element method, finite element method, etc.) should be used. Based on these methods, many studies have been carried out to improve the wave power conversion performance of the device, though it needs large quantities of grid data and a huge number of calculations. For example, to optimise the absorber's wave power conversion for a targeted location in the Atlantic off the west coast of Ireland, Goggins and Finnegan [16] introduced a methodology considering geometric configuration contrasts with massive hydrodynamic numerical calculations using ANSYS-AQWA. To systematically analyse the effects of the geometric constraints of an oscillating water column wave energy converter for power optimisation in irregular waves, Gomes et al. [17] calculated extensive hydrodynamic data using the BEM-based code WAMIT. Later, Koh et al. [18] conducted a multi-objective optimisation considering the constraints of PTO damping and the production cost of the required sheet plate volume. Because of the requirement for sufficient relevant hydrodynamic data corresponding to the power conversion of geometrical parameter selection, the commercial program ANSYS-AQWA was employed, which resulted in the establishment of a vast amount of grid data and models. Related float configuration optimisation research considering more complex structures and more advanced methods is still ongoing, such as by Garcia-Teruel et al. [19]-[20], Esmaeilzadeh et al. [21], Sergiienko et al. [22], Berenjkoob et al. [23], and Rodríguez et al. [24]. However, the researches on the influence of the PTO damping and

geometrical configurations on the power conversion of the harvesting buoy with heave motion are still not sufficiently thorough and comprehensive.

In this context, a semi-analytical solution, first put forward by Kokkinowrachos et al. [25] and explored further by Zhang et al. [10], was employed for the relatively fast and simple hydrodynamic calculation and systematic wave power conversion evaluation of a vertical axisymmetric absorber with heave motion. The lateral section shapes of the buoy were described by different power series equations, such as half for concave and one for conical. Having divided the fluid domain under the float into coaxial annular fluid domains, a general eigenfunction expansion matching method was then understandably employed. A convergence and accuracy test for the hydrodynamic calculation of a hemisphere was conducted by increasing the number of discretisations. Further, a set of hydrodynamic coefficients and wave excitation forces for the oscillating absorbers with continuous draught ratios were calculated conveniently. Then, the corresponding captured wave power in regular and irregular waves, considering the general and optimised PTO mechanical damping coefficients, was calculated. The effect of the geometrical configuration of the buoys on the wave power conversion was systematically analysed and evaluated, and can be referred to in future work to improve the wave energy conversion performance.

Table 1. Variables and their definitions

Variable	Definition	Variable	Definition
ω	Wave frequency (rad/s)	A	Wave amplitude (m)
$\ddot{O}$	Velocity potential (m^2/s)	g	Gravity acceleration (m/s^2)
h	Water depth (m)	m	Mass of the floater (kg)
k	Wave number	ρ	Water density (kg/m^3)
F_{d3}	Wave force in heave (N)	R	Radius of the floater (m)
μ_{33}	Added mass in heave (kg)	d	Draught of the floater (m)
λ_{33}	Radiated damping in heave (Ns/m)	t	Straight wall height of the floater (m)
k_{33}	Hydrostatic restoring stiffness coefficient (N/m)	η	Wave energy conversion efficiency
RAO_3	Response amplitude operator in heave	c_p	PTO damping coefficient (Ns/m)
$\overline{F}_{d3}$	Non-dimensional wave force in heave	P0	Incident wave power (W)
$\overline{\mu}_{33}$	Non-dimensional added mass in heave	Pa	Average captured wave power (W)
$\overline{\lambda}_{33}$	Non-dimensional radiated damping in heave	ω_p	Peak frequency (rad/s)
$S(\omega)$	Wave spectral density	H_S	Significant wave height (m)

HYDRODYNAMIC FORMULATIONS

The oscillating absorber considered in this study is shown in Fig. 1. We define the cylindrical coordinated system (r,θ,z) by its origin located at the centre of the absorber and on the mean plane of the free surface. The axis *oz* is vertically upward. The wetted surface of the absorber is assumed to comprise a cylindrical surface and a vertical axisymmetric curved surface. The outer radius of the two surfaces is the same and denoted as R. The cylinder height, the whole draught and the water depth are denoted as t, d and h, respectively, in which $0 \le t \le d$. For convenience, the variables and their definitions are displayed in Table 1.

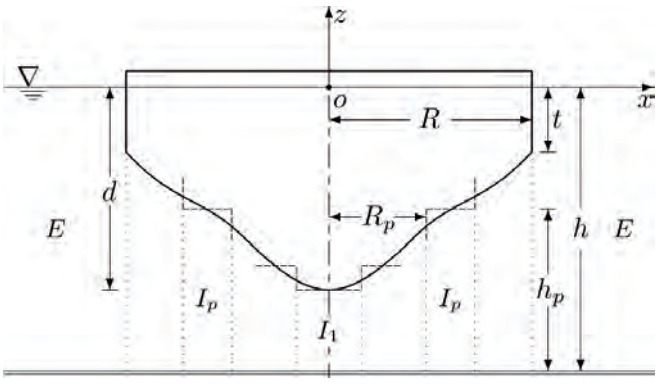

Fig. 1. Definition of fluid subdomains of boundary approximation method

For incompressible and inviscid fluid, and for small amplitude wave theory with irrotational motion, we can introduce a velocity potential $\Psi(r,\theta,z,t)$ to describe the fluid flow. Assuming harmonic motion in frequency domain, for the sake of simplicity, the time variation can be omitted and the velocity potential can be written as

$$\Psi(r,\theta,z,t) = \mathrm{Re}[\Phi(r,\theta,z)e^{-i\omega t}] \tag{1}$$

According to the line plane wave theory, the spatial velocity potential Φ can be decomposed as the undisturbed incident wave velocity potential Φ_0, scattered potential Φ_7 for a fixed body and radiation potential Φ_j(j = 1,3,5) induced by the body motion oscillation in otherwise calm water. The velocity potentials Φ_0 and Φ_7 comprise the diffracted potential $\Phi_D$around the structure with constraints. Then, we have

$$\begin{aligned}\Phi(r,\theta,z) &= \Phi_0(r,\theta,z) + \Phi_7(r,\theta,z) + \sum_{j=1}^{6} -i\omega\xi_j\Phi_j(r,\theta,z)\\ \Phi_D(r,\theta,z) &= \Phi_0(r,\theta,z) + \Phi_7(r,\theta,z)\end{aligned} \tag{2}$$

where ξ_j (j = 1-6) is the j-th mode motion amplitude and only $j = 3$ for heave is considered in this paper. The aforementioned velocity potentials should satisfy the
Laplace equation:

$$\nabla^2\Phi = 0 \tag{3}$$

free surface condition:

$$\omega^2\Phi - g\partial_z\Phi = 0 \quad z = 0, r \geq R \tag{4}$$

seabed condition:

$$\partial_z\Phi = 0 \quad z = -h \tag{5}$$

hull boundary condition:

$$\partial_n\Phi_3 = V_n, \quad \partial_n(\Phi_0 + \Phi_7) = 0 \tag{6}$$

radiation condition:

$$\lim_{r\to\infty}\sqrt{kr}(\partial_r\Phi - ik\Phi) = 0 \tag{7}$$

where i is an imaginary unit and k is the wave number, which comes from the dispersion relation, and the symbol $\partial_n()$ indicates the derivative in the normal vector pointing always outwards from the wetted surface of the device.

ADDED MASS, RADIATION DAMPING AND WAVE FORCING

Assuming that an undisturbed incident sinusoidal wave with amplitude A and frequency w propagates along the positive x-axis direction, this can be expressed in cylindrical coordinates as

$$\Phi_0(r,\theta,z) = \frac{Ag}{i\omega}\sum_{l=0}^{\infty}\varphi_{0\ell}(r,z)\cos\ell\theta \quad \text{with} \quad \varphi_{0\ell}(r,z) = \tag{8}$$

$$= \varepsilon_\ell i^\ell \mathbf{J}_\ell(kr)\cosh k(z+h)/\cosh kh$$

where $J_\ell(\cdot)$ is the Bessel function of the first kind, of order $\ell(\ell = 0,1,2,\cdots)$ and ε_ℓ is the Neumann symbol, defined by $\varepsilon_0 = 1$ and $\varepsilon_\ell = 2$ for $\ell \geq 1$. In accordance with , the velocity potential of the diffraction potential field caused by the fixed device can be written in the form

$$\Phi_7(r,\theta,z) = \frac{Ag}{i\omega}\sum_{\ell=0}^{\infty}\varepsilon_\ell i^\ell\varphi_{7\ell}(r,z)\cos\ell\theta \tag{9}$$

In the unbounded fluid domain with finite water depth, the radiation velocity potential caused by the forced oscillated vertical axisymmetric body in heave can be expressed as

$$\Phi_3(r,\theta,z) = \varphi_{3\ell}(r,z) \text{ with } \ell = 0 \tag{10}$$

The newly introduced velocity potential expressions $\varphi_{D\ell}$ and $\varphi_{3\ell}$ should also satisfy the former boundary conditions, and their solution will be the key problem in the hydrodynamic analysis of the oscillating buoy. To obtain the hydrodynamic characteristics of the absorbers, the velocity potentials around the vertical axisymmetric body should be confirmed. Before decomposing the Laplace equation with the method of separation of variables, we should first divide the fluid domain around the device into several subdomains. For the complex axisymmetric wetted surface, we decompose it into ring-shaped stepped surfaces by dividing the projection curve on the vertical plane averagely. Thus, the velocity potentials in each domain can be expressed in the form of Fourier series.

(a) Velocity potential in domain $E\,(r \geq R, -h \leq z \leq 0)$

$$\begin{aligned}\varphi_{j\ell}^E(r,z) &= \alpha_{j\ell 0}^E\Gamma_0(z)\mathbf{H}_\ell(k_0 r)/\mathbf{H}'_\ell(k_0 R) +\\ &+ \sum_{n=1}^{\infty}\alpha_{j\ell n}^E\Gamma_n(z)\mathbf{K}_\ell(k_n r)/\mathbf{K}'_\ell(k_n R) + \Re_{j\ell}^E(r,z)\end{aligned} \tag{11}$$

with $j = 3,7$, and $\mathbf{H}_\ell(\cdot)$ and $\mathbf{K}_\ell(\cdot)$ are the Hankel function of the first kind and the modified Bessel function of the second kind of order ℓ separately. Here and hereafter, a prime denotes taking the differentiation of a function with respect to its argument. The wave numbers k_0, $k_n(n = 1,2,3\cdots)$ are defined by $\omega^2 = gk_0\tanh k_0 h = -gk_n\tan k_n h$. The function expressions $\tilde{A}(\cdot)$ and $\Re(\cdot)$ are given as

$$\Gamma_0(z)=\cos k_0h\cosh k_0(z+h)/[2k_0h+\sinh 2k_0h]\quad \Gamma_n(z)=[\cos k_n(z+h)]/[2k_nh+\sin 2k_nh]$$
$$\Re^E_{30}(r,z)=0\quad \Re^E_{D\ell}(r,z)=[\cosh k_0(z+h)]/\cosh k_0h\,\varepsilon_\ell i^\ell \mathbf{J}_\ell(k_0r) \tag{12}$$

(b) Velocity potential in domain I_1 $(0\le r\le R_1,-h\le z\le h_1-h)$ and I_p $(2\le p\le N, R_{p-1}\le r\le R_p,-h\le z\le h_p-h)$

$$\varphi^{I_1}_{j\ell}(r,z)=\alpha^{I_1}_{j\ell0}G^{I_1}_{j\ell}(r)+\sum_{n=1}^{\infty}[\alpha^{I_1}_{j\ell n}\mathbf{I}_\ell(\lambda_{n1}r)/\mathbf{I}_\ell(\lambda_{n1}R_1)\cos\lambda_{n1}(z+h)]+\Re^{I_1}_{j\ell}(r,z) \tag{13}$$

$$\varphi^{I_p}_{j\ell}(r,z)=\alpha^{I_p}_{j\ell0}G^{I_p}_{j\ell}(r)+\sum_{n=1}^{\infty}\alpha^{I_p}_{j\ell n}Q^{I_p}_{n\ell}(r)\cos\lambda_{np}(z+h)+\tilde\alpha^{I_p}_{j\ell0}\tilde G^{I_p}_{j\ell}(r)+ +\sum_{n_p=1}^{\infty}\tilde\alpha^{I_p}_{j\ell n}\tilde Q^{I_p}_{n\ell}(r)\cos\lambda_{np}(z+h)+\Re^{I_p}_{j\ell}(r,z) \tag{14}$$

In the eigenfunction expansions for the velocity potentials, similarly, the unknown function expressions of λ, $G(\cdot)$, $Q(\cdot)$ and $\Re(\cdot)$ are given as

$$\Re^{I_p}_{D\ell}(r,z)=0,\ \Re^{I_p}_{30}(r,z)=[2(z+h)^2-r^2]/(4h_p)$$
$$\lambda_{np}=n\pi/h_p,\ G^{I_1}_{D\ell}(r)=(r/R_1)^\ell,\ G^{I_1}_{30}(r)=1$$
$$G^{I_p}_{j\ell}(r)=\begin{cases}\ln(r/R_{p-1})/\ln(R_p/R_{p-1})\\ [(r/R_{p-1})^\ell-(R_{p-1}/r)^\ell]/(R_p/R_{p-1})^\ell-(R_{p-1}/R_p)^\ell\end{cases}\quad p\ge2$$
$$\tilde G^{I_p}_{j\ell}(r)=\begin{cases}\ln(R_p/r)/\ln(R_p/R_{p-1})\\ [(R_p/r)^\ell-(r/R_p)^\ell]/[(R_p/R_{p-1})^\ell-(R_{p-1}/R_p)^\ell]\end{cases}\quad p\ge2 \tag{15}$$
$$Q^{I_p}_{n\ell}(r)=[\mathbf{K}_\ell(\lambda_{np}R_{p-1})\mathbf{I}_\ell(\lambda_{np}r)-\mathbf{K}_\ell(\lambda_{np}r)\mathbf{I}_\ell(\lambda_{np}R_{p-1})]/\mathbf{\Pi}_{p\ell n}\quad p\ge2$$
$$\tilde Q^{I_p}_{n\ell}(r)=[\mathbf{K}_\ell(\lambda_{np}r)\mathbf{I}_\ell(\lambda_{np}R_p)-\mathbf{K}_\ell(\lambda_{np}R_p)\mathbf{I}_\ell(\lambda_{np}r)]/\mathbf{\Pi}_{p\ell n}\quad p\ge2$$
$$\mathbf{\Pi}_{p\ell n}=\mathbf{K}_\ell(\lambda_{np}R_{p-1})\mathbf{I}_\ell(\lambda_{np}R_p)-\mathbf{K}_\ell(\lambda_{np}R_p)\mathbf{I}_\ell(\lambda_{np}R_{p-1})\quad p\ge2$$

The sets of unknown Fourier coefficients *a* are determined by taking advantage of orthogonality, in the so-called Garrett method, according to matching of the potentials and its normal derivative on the juncture boundaries surface shared by the subdomains. For the detailed matching procedure, the reader can refer to Zhang et al. [10]. Considering the heave motion applied in the wave energy conversion, the wave forcing and radiation damping coefficients in heave need to be obtained. Thus, by defining $R_0=0$, the non-dimensional wave excitation forces and hydrodynamic coefficients of the absorber in heave can be calculated and defined by

$$\begin{aligned}\bar F_{d3}&=\frac{F_{d3}}{\rho gAR^2}=-\frac{i2\pi}{R^2}\sum_{p=1}^{N}\int_{R_{p-1}}^{R_p}\varphi^{I_p}_{30}(r,h_p-h)rdr\\ &=-i\pi\alpha^{I_1}_{700}-\pi\sum_{n=1}^{\infty}\alpha^{I_1}_{70n}\frac{(-1)^n}{\lambda_{n1}R^2}\frac{\mathbf{I}_0(k_0r)}{\mathbf{I}'_0(k_0R)}\\ &\quad-\frac{i2\pi}{R^2}\sum_{p=2}^{N}\left\{\alpha^{I_p}_{700}[1-\frac{R_p^2-R_{p-1}^2}{2R_p^2\ln(R_p/R_{p-1})}]+\sum_{n=1}^{\infty}\alpha^{I_p}_{70n}(-1)^n\frac{R_pQ^{I_p}_{n0}(R_{p-1})}{\lambda_{np}}\right\}\\ &\quad-\frac{i2\pi}{R^2}\sum_{p=2}^{N}\left\{\tilde\alpha^{I_p}_{700}[\frac{R_{p-1}^2}{R_p^2}-\frac{R_p^2-R_{p-1}^2}{2R_p^2\ln(R_p/R_{p-1})}]+\sum_{n=1}^{\infty}\tilde\alpha^{I_p}_{70n}(-1)^n\frac{R_p\tilde Q^{I_p}_{n0}(R_{p-1})}{\lambda_{np}}\right\}\end{aligned} \tag{16}$$

$$\begin{aligned}\bar\mu_{33}+i\bar\lambda_{33}&=\frac{\mu_{33}}{\rho R^3}+i\frac{\lambda_{33}}{\rho\omega R^3}=-\frac{i2\pi d}{R^3}\sum_{p=1}^{N}\int_{R_{p-1}}^{R_p}\varphi^{I_p}_{30}(r,h_p-h)rdr\\ &=-\frac{i\pi d}{R}\alpha^{I_1}_{300}-\frac{\pi d}{R}\sum_{n=1}^{\infty}\alpha^{I_1}_{30n}\frac{(-1)^n}{\lambda_nR_1^2}\frac{\mathbf{I}_0(k_0r)}{\mathbf{I}'_0(k_0R)}\\ &\quad-\frac{i2\pi d}{R^3}\sum_{p=2}^{N}\left\{\alpha^{I_p}_{300}[1-\frac{R_p^2-R_{p-1}^2}{2R_p^2\ln(R_p/R_{p-1})}]+\sum_{n=1}^{\infty}\alpha^{I_p}_{30n}(-1)^n\frac{R_pQ^{I_p}_{n0}(R_{p-1})}{\lambda_{np}}\right\}\\ &\quad-\frac{i2\pi d}{R^3}\sum_{p=2}^{N}\left\{\tilde\alpha^{I_p,0}_{3}[\frac{R_{p-1}^2}{R_p^2}-\frac{R_p^2-R_{p-1}^2}{2R_p^2\ln(R_p/R_{p-1})}]+\sum_{n=1}^{\infty}\tilde\alpha^{I_p}_{30n}(-1)^n\frac{R_p\tilde Q^{I_p}_{n0}(R_{p-1})}{\lambda_{np}}\right\}\end{aligned} \tag{17}$$

WAVE ENERGY CONVERSION

Having obtained the hydrodynamic parameters and wave-excited forces, the wave energy conversion ability of the buoys can be further investigated. The power take-off (PTO) mechanism assembled between the absorber and the solid platform or seabed is composed of a linear damper, which can be activated to output electric energy under the absorber's heave reciprocating motion [26]. In such case, the motion of the buoy with the PTO mechanism in waves can be expressed as

$$(m+\mu_{33})\ddot z+(\lambda_{33}+c_p)\dot z+k_{33}z=f_{d3} \tag{18}$$

where c_p denotes the damper's damping coefficient, which can be regulated, k_{33} is the hydrostatic restoring stiffness coefficient and is expressed as ρgS, with water density ρ, gravity acceleration *g* and waterline area *S*. The variables $\ddot z$, $\dot z$, z and f_{d3} contain the common time factor $e^{i\omega t}$, which can be unified as $\phi=\Phi e^{-\omega t}$. By separating the time factor from these variables into the frequency domain, the response amplitude operator (RAO) of the buoy in heave can be obtained and given as

$$RAO_3=\frac{Z}{A}=\frac{F_{d3}}{-\omega^2(m+\mu_{33})+i\omega(\lambda_{33}+c_p)+k_{33}} \tag{19}$$

In this paper, the wave-excited motion amplitude *A* here is unit, so the calculated RAO will also be the motion amplitude. According to Falnes [28], for an oscillating-buoy wave energy converter, the captured wave energy with a linear PTO mechanism can be defined as

$$P_a=\int_{\Delta t}^{T+\Delta t}c_p\dot z\cdot\dot z dt=\frac{1}{2}c_p\omega^2Z^2 \tag{20}$$

Therefore, the optimal PTO damping coefficient can be obtained by solving the extreme value problem of the power expression about the damping coefficient. Then, we have the optimal expression of the damping coefficient:

$$c_{p,opt}=[\lambda_{33}^2+(\omega m+\omega\mu_{33}-\frac{k_{33}}{\omega})^2]^{1/2} \tag{21}$$

To better understand the wave conversion ability of the buoy with different geometries, we define the capture width ratio η to describe the wave energy conversion efficiency, expressed as

$$\eta = P_a / P_0 \tag{22}$$

with the incident wave power defined as

$$P_0 = \rho g B \omega A / (4k_0) \cdot (1 + 2k_0 h / \sinh 2k_0 h) \tag{23}$$

where B denotes the heave wave width of the buoy and is defined as twice the radius of the buoy in this paper. k_0 is the zero order wave number for a given wave frequency ω.

NUMERICAL RESULTS

CONVERGENCE AND VERIFICATION

The numerical work in this section is involved in the choice of the number of terms used in the infinite simulations. The former 30 terms of the unknown Fourier coefficients are adopted in the infinite summations to compute the numerical results because the infinite summations have excellent truncation characteristics, as depicted in Yeung [29]. A quintessential hemisphere with radius R=5m and draught 5 m in the water depth of $h = 50$ m with different incident wave frequencies is adopted here to verify the feasibility and validity of this semi-analytical solution.

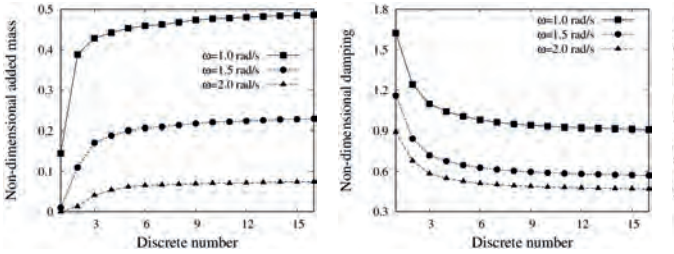

Fig. 2. Non-dimensional hydrodynamic calculation results with different incident wave frequencies for a hemisphere

The examinations on the convergence of the wave forces and hydrodynamic coefficients of the above-mentioned hemisphere in the presence of regular waves of different frequencies in a water depth of $h = 50$ m are shown in Fig. 2. It can be concluded that convergent results can be achieved when the number of discretization reaches 15.

The analytical solution method based upon the multipole theory for a hemisphere has been developed by Hulme [30]. In such case, the correctness of the present semi-analytical method can be verified by calculating the hydrodynamic parameters of the above-mentioned absorber with these two methods. Comparisons of the wave excitation forces and hydrodynamic coefficients of the absorber in heave in Table 2 show good agreement, which can be regarded as validation of the present method.

Tab. 2. Verification of the solution method

Frequency (rad/s)	1.0		1.5		2.0	
Method	Present	Analytical	Present	Analytical	Present	Analytical
$F_{d3}/(\rho g A R^2)$	0.9925	0.9895	0.3736	0.3745	0.1388	0.1367
$\mu_{33}/(\rho R^3)$	0.488	0.4903	0.2311	0.2297	0.0756	0.0763
$\lambda_{33}/(\rho R^3 \omega)$	0.9058	0.9042	0.5676	0.5667	0.4668	0.4701
Maximum error (%)	0.47		0.61		1.54	

HYDRODYNAMIC PERFORMANCE

Based upon the above verified hydrodynamic calculation method, the hydrodynamic characteristics of the vertical axisymmetric absorbers can be analysed. In such case, four kinds of vertical axisymmetric absorbers are considered for evaluation of the influence of the geometry on the hydrodynamic characteristics and wave energy conversion performance. The complex wetted surface of the absorber comprises a vertical cylindrical surface and a vertical axisymmetric curved surface. The geometrical parameters and lateral views of the absorbers are shown in Fig. 3. They are concave, conical, parabolic and ellipsoidal surfaces, and we define them in turn as cases 1–4, respectively. The curves in the semi-section lateral views in the dashed frames are described with curvilinear equations in their local coordinate systems as

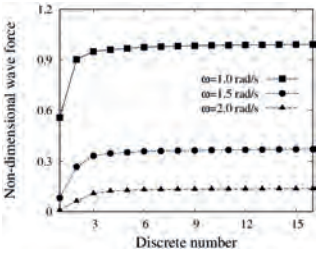

$$\begin{aligned} &\text{Case } 1 \rightarrow z/(d-t) = \sqrt{x/R} \\ &\text{Case } 2 \rightarrow z/(d-t) = x/R \\ &\text{Case } 3 \rightarrow z/(d-t) = (x/R)^2 \\ &\text{Case } 4 \rightarrow z/(d-t) = 1 - \sqrt{1-(x/R)^2} \end{aligned} \tag{24}$$

in which $0 \le x \le R$, $0 \le t < d$, and, to describe the absorber's geometrical characteristics more conveniently, we define the draught ratio $(d-t)/d$ as $d_r (0 \le d_r \le 1)$. When the draught ratio equals 0, the absorbers will be vertical truncated cylinders. In addition, the buoys are defined as concave, conical, paraboloid and ellipsoid buoys in turn.

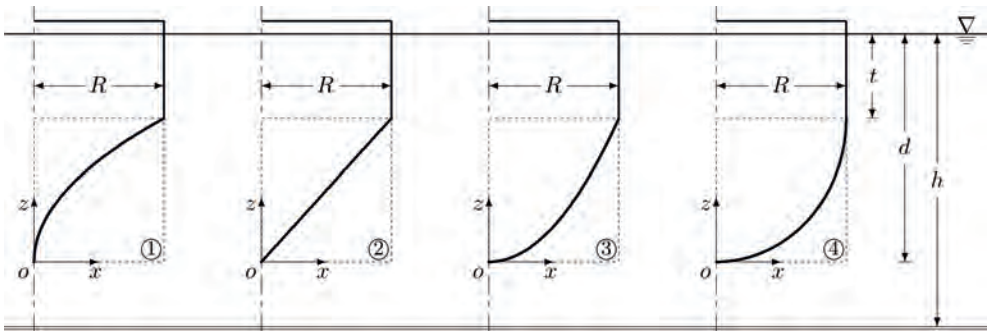

Fig. 3. Geometrical parameters description and semi-section lateral views of the considered absorbers

In this paper, we define the four types of buoys with the same outer radius $R = 5$ m and draught $d = 6$ m, in water with depth $h = 50$ m, to estimate the hydrodynamic and wave power conversion performance impartially. The response amplitude operators of the buoys in heave motion with free vibration, considering consecutive incident wave frequencies and draught ratios, are given in Fig. 4. It can be clearly seen that the motion RAOs in heave for the chosen absorbers have nearly identical trends to the incident wave frequencies and draught ratios. For a given draught ratio, there will be a peak value of the RAO with the increase of wave frequencies. However, in the range of the draught ratios, the concave type buoy shows a relatively high-frequency bandwidth, and when the draught ratio reaches 0.8, the resonance characteristics are not so obvious. In such case, the motion characteristics, as well as their formation mechanism at higher draught ratios, take on added importance. For a better understanding, the heave RAO and hydrodynamic parameters are also described with the given draught ratio equal to 0.8 and 1.0 for the four kinds of buoys.

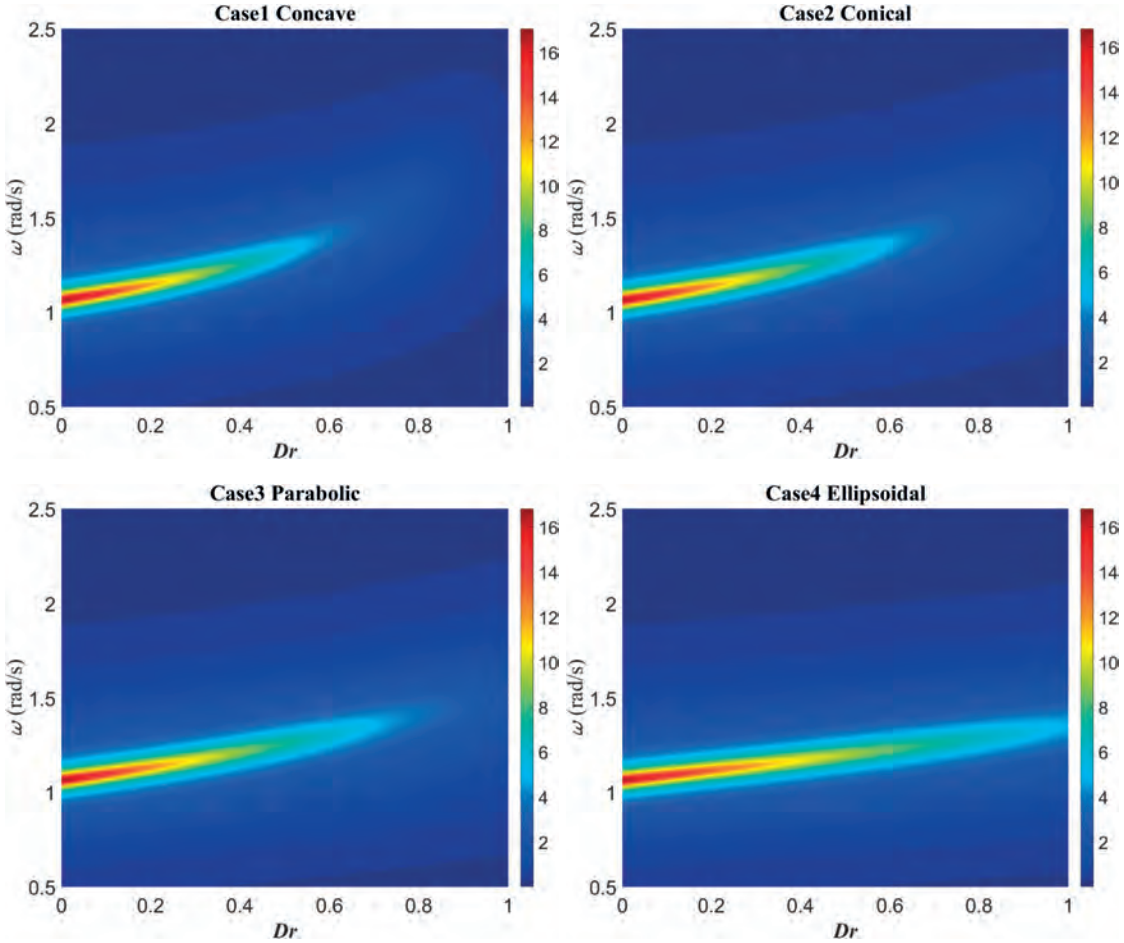

Fig. 4. Heave RAOs of the absorbers with free vibration

As shown in Fig. 5, the heave RAOs of the concave and conical buoys have no obvious peak characteristics, as well as corresponding wave-excited forces. With the increase of the draught ratio, the vertical component of the velocity potential gradient at the bottom of the float decreases, and the resulting heave excitation force also decreases. However, the radiated velocity potential comes from the forced motion of the buoys in quiescent water. The non-planar bottom caused by the draught ratio increases the external energy transfer of the radiation wave. Thus, the radiated wave forces increase along with the increase of the draught ratio. These two reasons cause the motion response of the buoys to slow down.

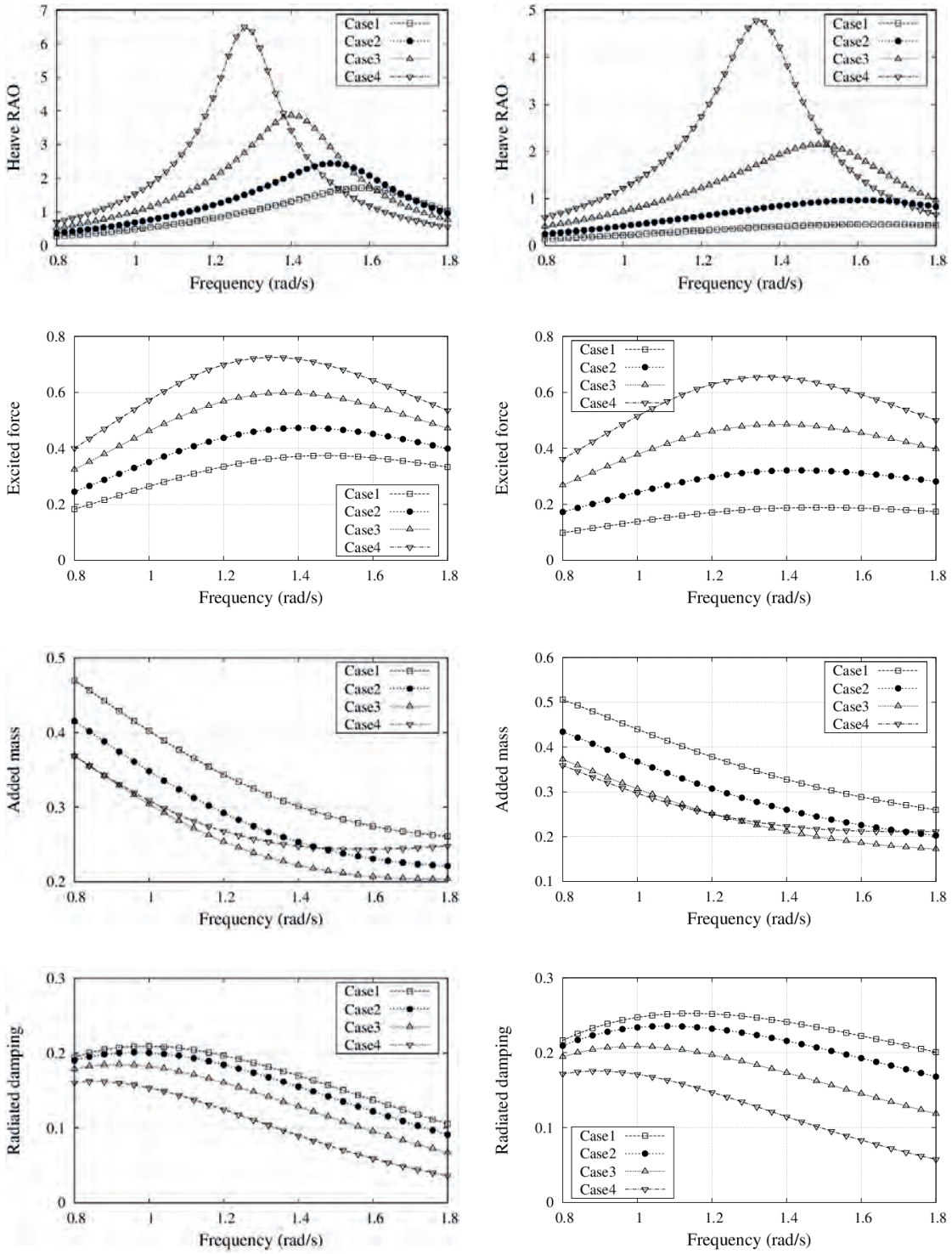

Fig. 5. Motion RAOs, excited forces, added mass and radiated damping of the absorbers in heave with dr equal to 0.8 (left) and 1.0 (right)

In addition, the motion response and hydrodynamic parameters of the floating buoys at their natural frequencies have also changed greatly. The natural frequencies of the buoys with different draught ratios are described in Table 3. Compared with the truncated cylinder, the natural frequencies of the four types of buoys are increased, and with the increase of the draught ratio, the range of increase is more obvious. In fact, this phenomenon can be explained by the wave excitation force and hydrodynamic parameters of the buoys at the natural frequency depicted in the following Fig. 6.

Tab. 3 Natural frequencies of the absorbers with free vibration

Case No.	Draught ratio					
	0.0	0.2	0.4	0.6	0.8	1.0
1	1.06	1.15	1.25	1.40	1.59	1.62
2	1.06	1.14	1.24	1.36	1.51	1.61
3	1.06	1.13	1.21	1.30	1.41	1.50
4	1.06	1.12	1.17	1.23	1.29	1.35

The natural frequencies of the free oscillating buoys are mainly decided by the generalised mass m, the stiffness coefficient k in heave and the damping coefficient c, which can be expressed as $\omega_n = \sqrt{k/m - (c/2m)^2}$. Since the four types of buoys have the same radius, the stiffness coefficient is the same. The depicted hydrodynamic parameters of the buoys with different draught ratios have little difference. The added mass of the conical and parabolic buoys even alternates. Therefore, the concave buoy with the minimum displacement has the maximum natural frequency. The motion response and wave-excited forces of the buoys at their natural frequencies are also given in Fig. 7. Both of them decrease with the increase of draught ratios. However, the motion response decreases rapidly and then flattens out, while the wave excitation force is the opposite, flattening out and then decreasing rapidly.

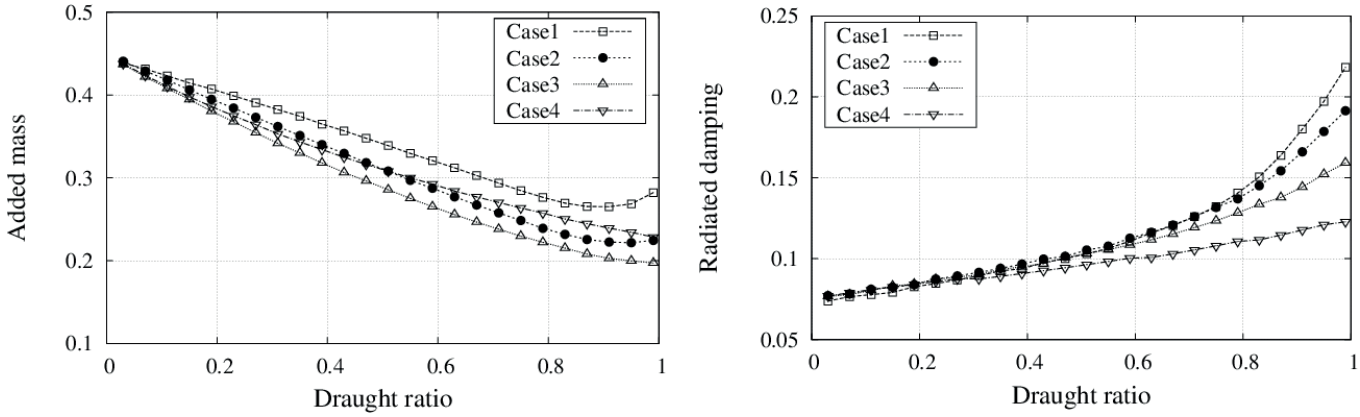

Fig. 6. Added mass and radiated damping in heave at natural frequencies of the free vibration absorbers

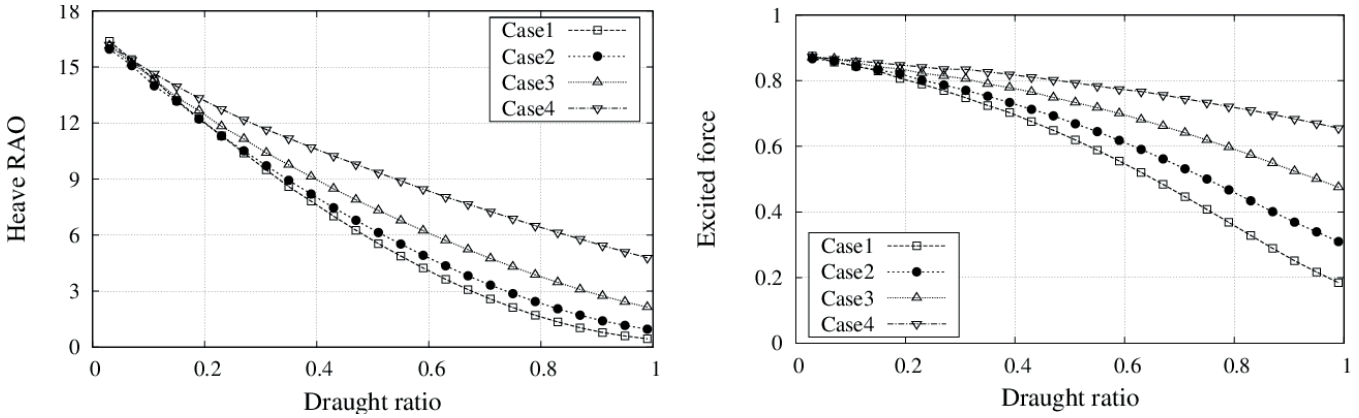

Fig. 7. Heave RAOs and excited forces at natural frequencies of the free vibration absorbers

WAVE ENERGY CONVERSION IN REGULAR WAVES

This section deals with the wave energy conversion ability of the four kinds of absorbers considered, based on the formal hydrodynamic parameters obtained. As has been mentioned before, the shape geometries of the buoys are the main factors in exploring the wave conversion characteristics. We therefore explore their effects on the natural frequencies of the buoys, which are partly decided by the viscous damping. In addition, the wave energy conversion of the buoy shows the optimal ability at the resonance frequency referring to Zhang et al. [10]. As shown in Fig. 8, the wave energy conversion efficiency of the chosen buoys with different draught ratios and PTO damping coefficients at their natural frequencies is explored and presented. For a given draught ratio, there will be a peak value of the capture width ratio with the increasing PTO damping coefficients. However, the increase of the draught ratios makes the peak value most outstanding for the ellipsoidal buoy.

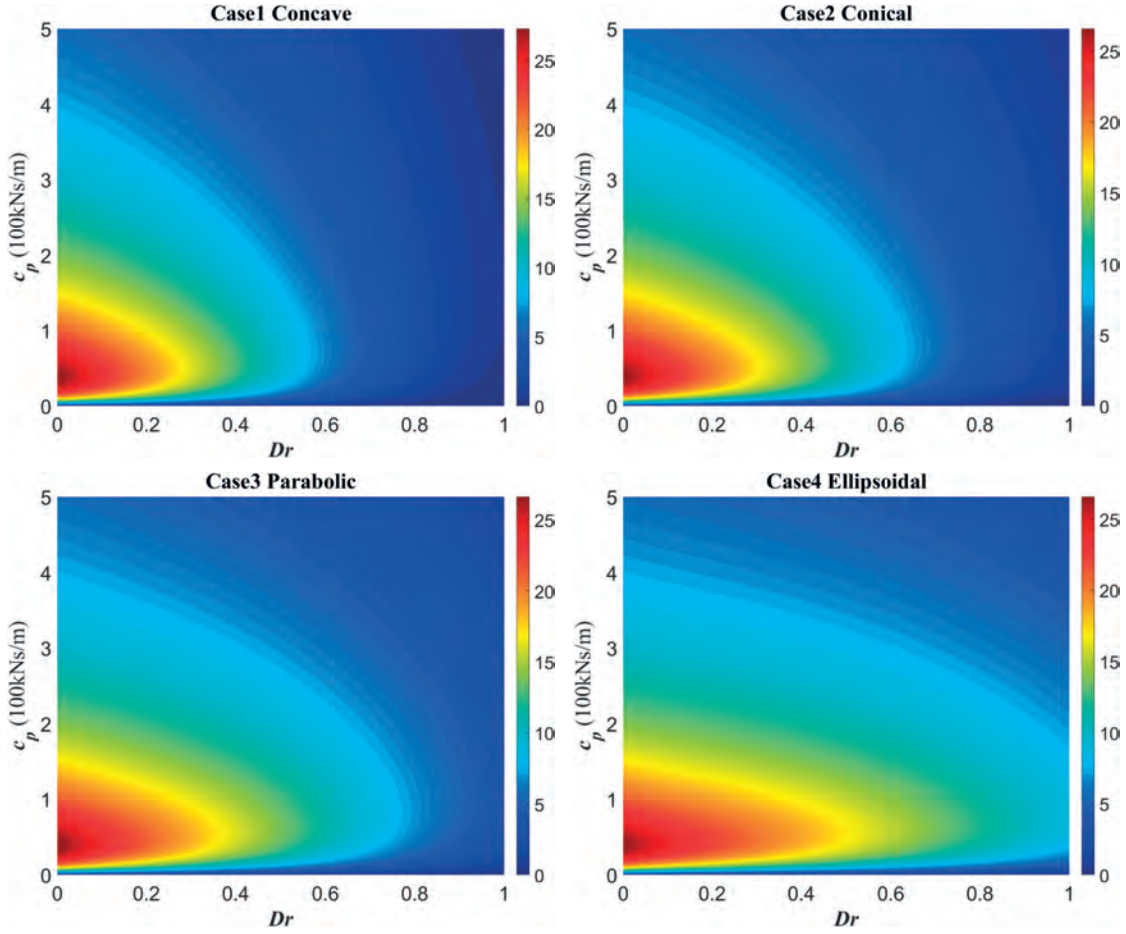

Fig. 8. Capture width ratios of the damped vibration absorbers at resonance frequencies

Of all the shapes and draught ratios, the truncated cylinder seems to have the best wave conversion ability though it may also have the narrowest frequency bandwidth. In such case, the wave energy conversion efficiency only reflects these absorbers' potential to convert waves at the resonance frequency. The conversion abilities in the whole incident wave frequency range, as well as the bandwidths of the buoys, need to be explored. For the convenience of research and description, we assume that the PTO mechanisms in this paper are adjustable and that the optimal state can be realised. Thus, the motion responses and wave capture efficiencies of the buoys with any given incident wave frequencies can be easily obtained and are depicted in the following Fig. 9.

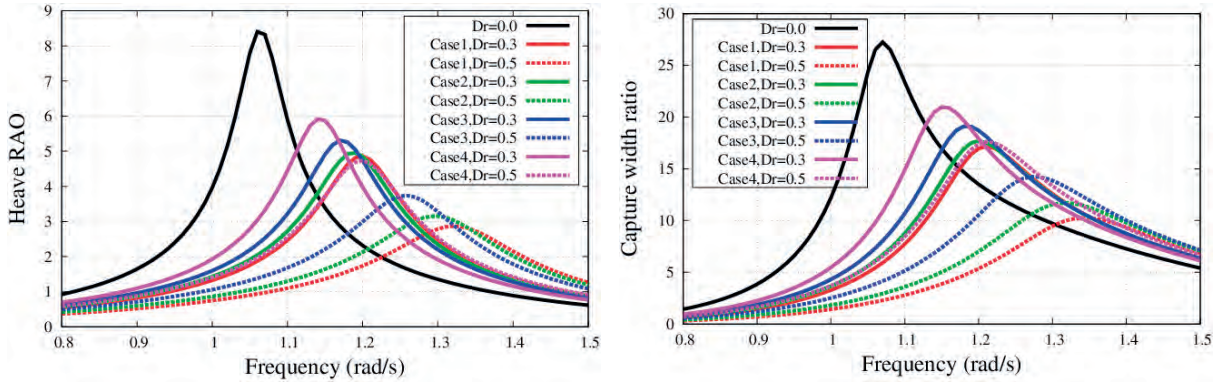

Fig. 9. Heave RAOs and capture width ratios of the damped vibration absorbers with optimal PTO damping coefficients

As shown in Fig. 9, the trend consistency between the motion response and wave power capture means that both the heave RAO and the capture width ratios for the considered shape geometries reach the optimal results at the natural frequencies. The increased draught ratios of the buoys not only decrease the optimal motion response and capture width ratio, but also increase the natural frequencies of the buoys. Though the truncated cylinder shows the best wave energy capture capability at natural frequency, its disadvantage in frequency bandwidth is also exposed. Here, the frequency bandwidth ω_{bf} is defined as the frequency range where the capture width ratios are more than half of the peak value.

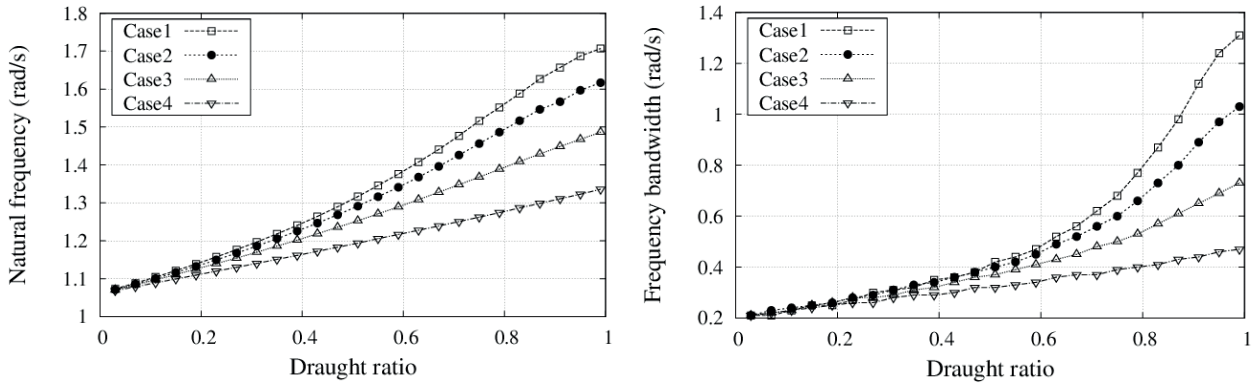

Fig. 10. Natural frequencies and frequency bandwidths of the damped vibration absorbers with optimal PTO damping coefficients

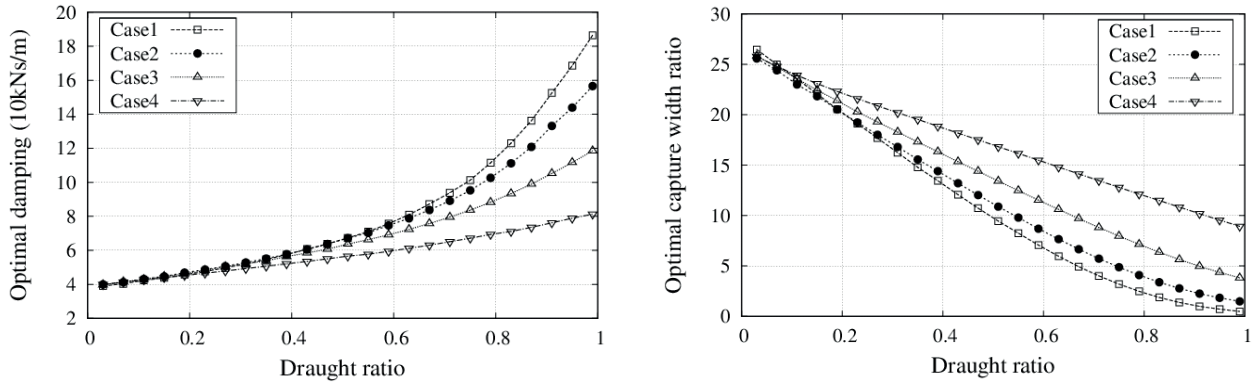

Fig. 11. Optimal PTO damping coefficients and capture width ratios of the damped vibration absorbers at natural frequencies

The natural frequencies and frequency bandwidth of the buoys with optimal PTO damping coefficients are shown in Fig. 10. It can be clearly observed that the increased draught ratio can increase the natural frequency effectively for a given shape of buoy. This conclusion can effectively improve the applicability of a buoy or beacon light to different sea areas. In addition, the concave buoy has the maximal natural frequency for a given draught ratio because of its decreased displacement. Though the concave buoy has the lowest wave conversion efficiency, it has the largest frequency bandwidth for a given draught, especially when the draught ratio is close to one. It is noteworthy that the natural frequencies and bandwidth are almost linear to the draught ratio, which is also presented in the optimal PTO damping coefficients and capture width ratios of the ellipsoidal buoy shown in Fig. 11. Special attention should also be given to the PTO mechanism, that the optimal damping coefficients and the relative optimal wave conversion efficiencies represent an obvious inverse correlation. In addition, a similar phenomenon also occurs between the frequency bandwidth and wave energy conversion efficiency.

To further explore the effect of the geometry and shape on the wave power conversion ability and eliminate the influence of the drainage volume difference at the same time, buoys with the same displacement are considered and the ellipsoidal buoy with a draught ratio equal to 1 is regarded as the reference criterion for displacement. In such case, the draught ratios of the concave, conical and parabolic buoys will be 0.417, 0.5 and 0.667, respectively. The calculation results of the buoys with the same displacement are given in Table 4. It can be observed that the natural frequencies of the forced vibrated buoys with optimal PTO damping coefficients have only a small difference. It should be stressed that, for the given four kinds of absorber, there is a perfect inverse correlation between the frequency bandwidth and the capture width ratios. This means that, though the shapes of the buoys are different, when their radius, draught and displacement are identical, the adaptabilities of their wave transformation have similar advantages. Certainly, this conclusion comes from the adjustability assumption of the optimal PTO damping coefficients for any given wave frequency. To further evaluate their wave conversion abilities, the irregular wave condition should be considered.

Tab. 4. Resonance and wave energy conversion characteristics of the buoys with same displacement

Case No.	Draught ratio	Natural frequency (rad/s)	Bandwidth (rad/s)	Optimal damping (10 kNs/m)	Optimal capture width ratio
1	0.417	1.258	0.36	5.960	12.413
2	0.500	1.286	0.40	6.587	11.196
3	0.667	1.328	0.45	7.575	9.702
4	1.000	1.339	0.48	8.211	8.786

WAVE ENERGY CONVERSION IN IRREGULAR WAVES

The above overall numerical results come from the assumption that the PTO damping can be adjusted to the optimal condition for a given incident wave frequency. However, in the real sea environment, a wave farm is complex and the frequencies are not isolated. In such case, the wave energy conversion abilities of buoys with manifold geometries and shapes should be further explored and evaluated. In this work, the JONSWAP spectrum [31] is selected to describe the incident wave spectrum and defined as

$$S(\omega)=\frac{\alpha g^2}{\omega^5}\exp\left\{-1.25(\omega_p/\omega)^4\right\}\cdot\gamma^{\exp\left\{-0.5(\omega-\omega_p/\sigma\omega_p)^2\right\}} \quad (25)$$

with

$$\begin{aligned}&\alpha=5.061(\frac{\omega_p}{2\pi})^4 H_s^2(1-0.287\log\gamma)\\&\sigma=0.07\quad \omega<\omega_p\\&\sigma=0.09\quad \omega\geq\omega_p\end{aligned} \quad (26)$$

where ω_p and H_s are the peak frequency and significant wave height, respectively. The peak elevation parameter γ is constant and typically given as 3.3 [26], whereas ω is the general incident wave frequency. As the axial-symmetric floater is not sensitive to the wave direction, the directional spectrum is not introduced here. According to the above wave absorption function , the converted wave power for the buoy in irregular waves can be obtained and expressed as

$$P_{am}=\int_0^{+\infty} c_p\omega^2\left|RAO(\omega)\right|^2 S(\omega)d\omega \quad (27)$$

Similarly, the inserted wave power for irregular waves can also be obtained according to function and given as

$$\begin{aligned}&P_{0m}=\int_0^{+\infty}\rho gBS(\omega)V(\omega)d\omega\\&V(\omega)=\omega/(4k_0)\cdot(1+2k_0h/\sinh 2k_0h)\end{aligned} \quad (28)$$

Then, the capture width ratio η_m of the buoy in irregular waves can be given as

$$_m \quad P_{am}/P_{\ m} \quad (29)$$

In such case, the optimal PTO damping and corresponding optimal capture width ratios can also be obtained by setting the partial derivative of the capture width ratio to the damping as zero. However, the motion RAOs of the buoys are also the implicit equations about the PTO damping coefficients. In such case, in this paper, the golden section search method [27] is employed to search for the optimal PTO damping coefficients for given peak frequencies and draught ratios.

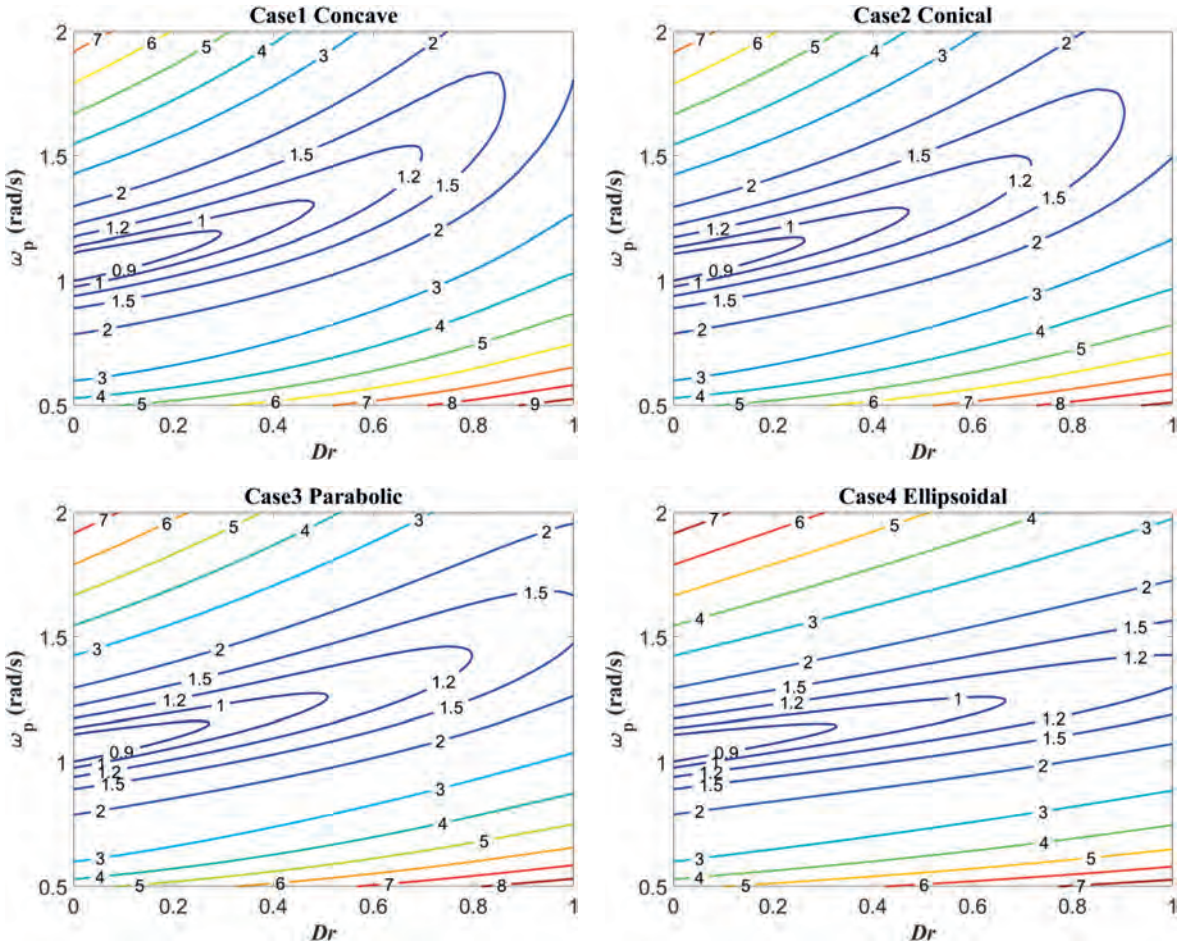

Fig. 12. Optimal PTO damping coefficients of the damped vibration absorbers at given peak frequencies ω_p and draught ratio D_r

The optimal PTO damping coefficients (100 kNs/m) for various peak frequencies and draught ratios are shown in Fig. 12. The display area of the optimal PTO damping coefficients is divided into two parts by the minimum values for the given draught ratios and peak frequencies. In the upper part, the optimal PTO damping coefficients increase with the increased peak frequencies and decreased draught ratios, while in the lower part, the coefficients show the opposite trend. From the former section in regular waves, we know that the change characteristics of the PTO damping coefficients can reflect the changing trend of energy capture to a certain extent. In such case, in real wave power conversion, the installed capacity of the device should be considered, combining the PTO mechanism and power capture. Because the PTO damping forces are limited by the hydraulic capacity or the resistive load, in this case, when the optimal PTO damping coefficients are obtained, the damping mechanism can be easily designed. The wave power capture of the buoys with optimal PTO damping coefficients in irregular wave is further explored and shown in Fig. 13. Similarly, for a given draught ratio, the capture width ratio first increases and then decreases with the increasing peak frequencies. And without considering the viscous resistance of the sea water, the truncated cylinder shows the highest wave conversion efficiency at a peak frequency equal to 1.07 rad/s. This means that, for a given working area, when the wave statistics are relatively stable and the matched wave spectrum is confirmed, the truncated cylindrical wave power absorber can be optimal, such as the 1.07 rad/s peak frequency in this paper. However, when the wave spectrum and its parameters are not stable and confirmed, the conical absorber may be the best choice for wave power conversion. For a better understanding of the effect of the geometry on the power conversion ability, buoys with the same displacement ratio are further explored. The displacement ratio here means the ratio of the absorber's displacement to that of the truncated cylinder with the same radius and draught.

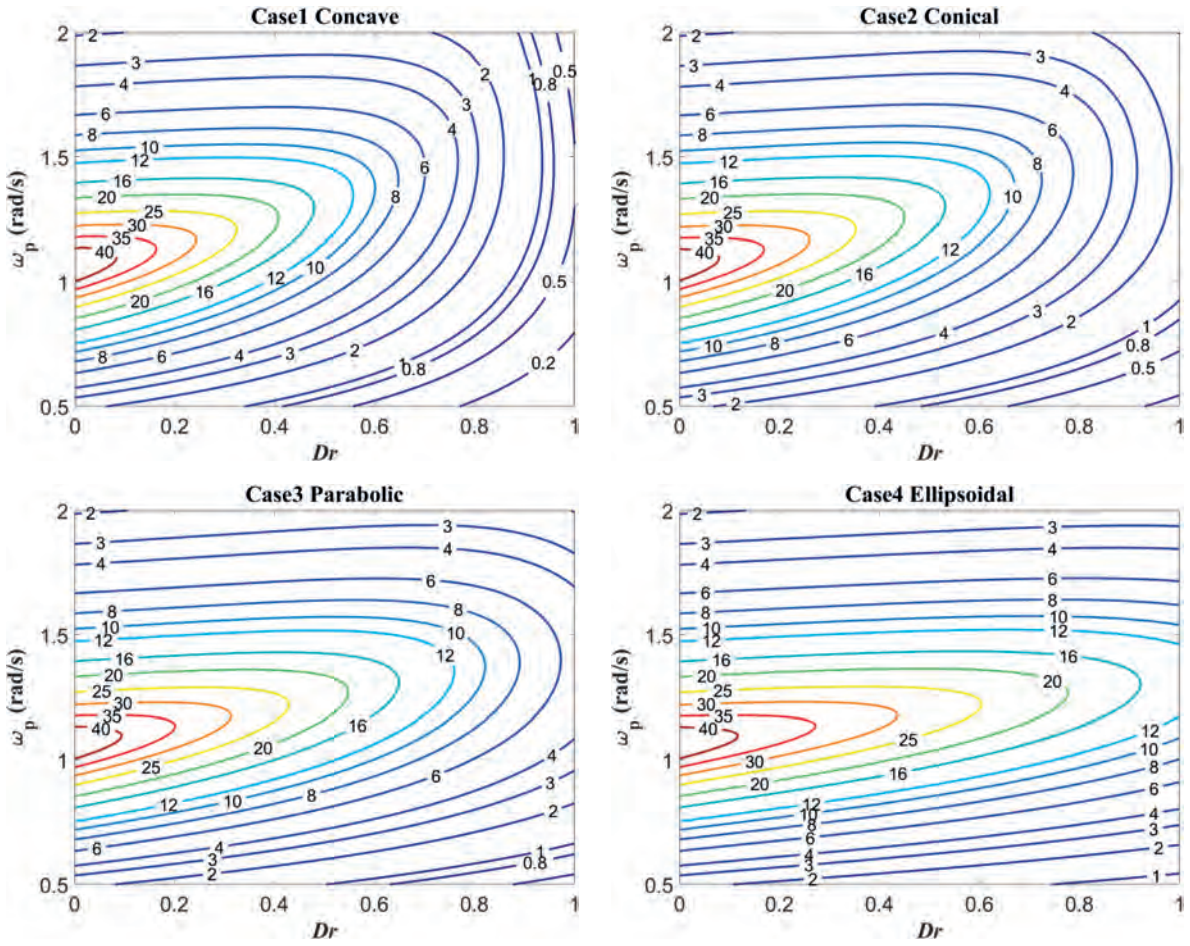

Fig. 13. Optimal capture width ratios of the damped vibration absorbers at given peak frequencies ω_p and draught ratio D_r

As shown in Fig.14, the optimal capture width ratios of the buoys with peak frequencies and displacement ratios are calculated and depicted, respectively. For different buoys with the same given displacements, the optimal capture width ratios both increase first and then decrease with the peak frequencies. However, before the capture width ratio reaches the peak value, the buoys with the same largest displacement have a better wave power conversion ability, and the concave buoy shows the best performance on the wave absorption. In addition, for the given shaped buoy with different displacements, the larger the displacement is, the better the power conversion will be. Taking the concave buoy as an example, when the peak frequency is 1.0 rad/s, the capture width ratio decreases from 28.1 when V_r is 0.9 to 12.7 when V_r is 0.7. The peak value also decreases from 37.4 to 22.1. However, it is worth noting that the relative peak frequency where the peak value occurs increases from 1.09 rad/s to 1.24 rad/s.

The buoys with different shapes and the same displacement also show interesting characteristics that the peak frequencies where the peak values occur increase in turn from the concave to the ellipsoidal buoy, and the smaller the displacement ratio, the more obvious the increase. In addition, for a given displacement, when the peak frequency reaches a certain value, the buoys with different shapes start to converge and show the same wave conversion ability. We call this particular peak frequency the assimilation frequency ω_a. It decreases with the increased displacement ratio. This means that, for a given working sea area, when the statistical wave is sure, we can choose the optimal buoy and the displacement to obtain the best wave absorption.

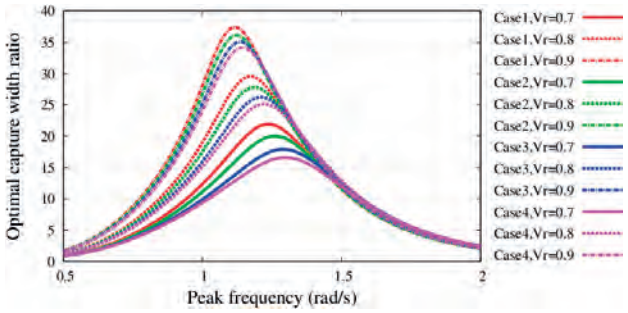

Fig. 14. Optimal capture width ratios of the damped vibration absorbers with peak frequencies ω_p at given displacement ratio V_r

DISCUSSION AND CONCLUSIONS

Four types of absorbers with different draught and displacement ratios are examined to analyse the effect of their geometries on the wave energy conversion ability, in which a semi-analytical method of decomposing the vertical axisymmetric curved surface into several ring-shaped stepped surfaces is introduced and examined. Combined with the updated body boundary characteristic, using the eigenfunction expansion matching method, the expressions of velocity potential in each domain, the added mass, radiation damping coefficients and wave-exciting forces of the oscillating buoy were obtained. The calculation results show that:

(1) The semi-analytical method by which the vertical axisymmetric curved surface is decomposed into several ring-shaped stepped surfaces can calculate accurately and investigate systematically the effect of the geometries on the hydrodynamic characteristics.

(2) In regular waves, the ellipsoidal buoy shows better wave energy conversion performance when the draught ratio reaches a relatively high value. In addition, its natural frequencies and bandwidth are almost linear to the draught ratio, as well as the optimal PTO damping coefficients and capture width ratios. When the draught ratios of all the four shaped buoys increase, their optimal motion responses, capture width ratios and natural frequencies also increase. Though the truncated cylinder shows the best wave energy capture capability at natural frequency, its disadvantage in frequency bandwidth is also exposed. The concave buoy has the maximal natural frequency for a given draught ratio because of its decreased displacement. In addition, though it has the lowest wave conversion efficiency, it has the largest frequency bandwidth for a given draught, especially when the draught ratio is close to one.

(3) In irregular waves, for a given draught ratio, the capture width ratios of all the considered shaped buoys first increase and then decrease with the increasing peak frequencies. Without considering the viscous resistance of the sea water, for a given working area, when the wave statistics are relatively stable and the matched wave spectrum is confirmed, the truncated cylindrical wave power absorber can be optimal. However, when the wave spectrum and its parameters are not stable and confirmed, the conical absorber may be the best choice for the wave power conversion.

(4) In irregular waves, when the displacements of the buoys are the same, the optimal capture width ratios both increase first and then decrease with the peak frequencies. However, before the capture width ratio reaches the peak value, the buoys with the same largest displacement have better wave power conversion ability and the concave buoy shows the best performance on the wave absorption. In addition, the peak frequencies where the peak values occur increase in turn from the concave to the ellipsoidal buoy, and the smaller the displacement ratio, the more obvious the increase.

(5) In irregular waves, for a given displacement, when the peak frequency reaches a certain value, the buoys with different shapes start to converge and show the same wave conversion ability. The assimilation frequency ω_a decreases with the increased displacement ratio, which means that, for a given working sea area, when the statistical wave is sure, we can choose the optimal buoy and the displacement to obtain the best wave absorption.

ACKNOWLEDGEMENTS

This paper is financially supported by the National Natural Science Foundation of China (No.51909111) and Natural Science Foundation of Jiangsu Province (No. BK20180980).

REFERENCES

1. F. Barbariol, A. Benetazzo, S. Carniel, and M. Sclavo, "Improving the assessment of wave energy resources by means of coupled wave-ocean numerical modeling," *Renewable Energy*, vol. 60, pp. 462-471, 2013.

2. L. Brik, "Application of constrained multi-objective optimization to the design of offshore structure hulls," *Journal of Offshore Mechanics and Arctic Engineering*, vol. 131, no. 1, p. 011301, 2009.

3. M. Liao, Y. Zhou, Y. Su, Z. Lian, and H. Jiang, "Dynamic analysis and multi-objective optimization of an offshore drilling tube system with pipe-in-pipe structure," *Applied Ocean Research*, vol. 75, pp. 85-99, 2018.

4. W. Lai, D. Li, and Y. Xie, "Simulation and experimental study of hydraulic cylinder in oscillating float-type wave energy converter," *Polish Maritime Research*, vol. 27, no. 2, pp. 30-38, 2020.

5. W. Lai, Y. Xie, and D. Li, "Numerical study on the optimization of hydrodynamic performance of oscillating buoy wave energy converter," *Polish Maritime Research*, vol. 28, no. 1, pp. 48-58, 2021.

6. E. Homayoun, H. Ghassemi, and H. Ghafari, "Power performance of the combined monopile wind turbine and floating buoy with heave-type wave energy converter," *Polish Maritime Research*, vol. 26, no. 3, pp. 107-114, 2019.

7. S. A. Mavrakos and G. M. Katsaounis, "Effects of floaters' hydrodynamics on the performance of tightly moored wave energy converters," *IET Renewable Power Generation*, vol. 4, no. 6, pp. 531-544, 2009.

8. A. P. McCabe, G. A. Aggidis, and M. B. Widden, "Optimizing the shape of a surge-and-pitch wave energy collector using a genetic algorithm," *Renewable Energy*, vol. 35, no. 12, pp. 2767-2775, 2010.

9. A. P. McCabe, "Constrained optimization of the shape of a wave energy collector by genetic algorithm," *Renewable Energy*, vol. 51, pp. 274-284, 2013.

10. W. Zhang, H. Liu, L. Zhang, and X. Zhang, "Hydrodynamic analysis and shape optimization for vertical axisymmetric wave energy converters," *China Ocean Engineering*, vol. 30, no. 6, pp. 954-966, 2016.

11. M. Shadman, S. F. Estefen, C. A. Rodriguez, and I. C. M. Nogueira, "A geometrical optimization method applied to a heaving point absorber wave energy converter," *Renewable Energy*, vol. 115, pp. 533-546, 2018.

12. S. Esmaeilzadeh and M. R. Alam, "Shape optimization of wave energy converters for broadband directional incident waves," *Ocean Engineering*, vol. 174, pp. 186-200, 2019.

13. I. O. Erselcan and A. Kükner, "A parametric optimization study towards the preliminary design of point absorber type wave energy converters suitable for the Turkish coasts of the Black Sea," *Ocean Engineering*, vol. 218, pp. 108275, 2020.

14. S. A. Mavrakos, "Hydrodynamic coefficients in heave of two concentric surface-piercing truncated circular cylinders," *Applied Ocean Research*, vol. 26, pp. 84-97, 2004.

15. E. E. Bachynskia, Y. L. Young, and R. W. Yeung, "Analysis and optimization of a tethered wave energy converter in irregular waves," *Renewable Energy*, vol. 48, pp. 133-145, 2012.

16. J. Goggins and W. Finnegan, "Shape optimisation of floating wave energy converters for a specified wave energy spectrum," *Renewable Energy*, vol. 71, pp. 208-220, 2014.

17. R. P. F. Gomes, J. C. C. Henriques, L. M. C. Gato, and A. F. O. Falcão, "Hydrodynamic optimization of an axisymmetric floating oscillating water column for wave energy conversion," *Renewable Energy*, vol. 44, pp. 328-339, 2012.

18. H. J. Koh, W. S. Ruy, I. H. Cho, and H. M. Kweon, "Multi-objective optimum design of a buoy for the resonant-type wave energy converter," *Journal of Marine Science and Technology*, vol. 20, no. 1, pp. 53-63, 2014.

19. A. Garcia-Teruel, B. DuPont, and D. I. M. Forehand, "Hull geometry optimization of wave energy converters: On the choice of the optimization algorithm and the geometry definition," *Applied Energy*, vol. 280, p. 115952, 2020.

20. A. Garcia-Teruel and D. I. M. Forehand, "A review of geometry optimization of wave energy converters," *Renewable and Sustainable Energy Reviews*, vol. 139, p. 110593, 2021.

21. S. Esmaeilzadeh and M. R. Alam, "Shape optimization of wave energy converters for broadband directional incident waves," *Ocean Engineering*, vol. 174, no. 15, pp. 186-200, 2019.

22. N. Y. Sergiienko, M. Neshat, L S. P. da Silva, B. Alexander, and M. Wagner., "Design optimisation of a multi-mode wave energy converter," in *Proc. of the 2020 39th International Conference on Ocean, Offshore and Arctic Engineering*, *2020*, *Online Virtual*.

23. M. N. Berenjkooba, M. Ghiasi, and C. G. Soares, "Influence of the shape of a buoy on the efficiency of its dual-motion wave energy conversion," *Energy*, vol. 214, p. 118998, 2021.

24. A. Claudio, C. A. Rodríguez, P. Rosa-Santos, and F. Taveira-Pinto, "Hydrodynamic optimization of the geometry of a sloped-motion wave energy converter," *Ocean Engineering*, vol. 199, p. 107046, 2020.

25. K. Kokkinowrachos, S. A. Mavrakos, and S. Asorakos, "Behavior of vertical bodies of revolution in waves," *Ocean Engineering*, vol. 13, no. 6, pp. 505-538, 1986.

26. M. Lopez, F. Taveira-Pinto, and P. Rosa-Santos, "Influence of the power take-off characteristics on the performance of CECO wave energy converter," *Energy*, vol. 120, pp. 686-697, 2017.

27. J. A. Koupaei, S. M. M. Hosseini, and F. M. Maalek Ghaini, "A new optimization algorithm based on chaotic maps and golden section search method," *Engineering Applications of Artificial Intelligence*, vol. 50, pp. 201-214, 2016.

28. J. Falnes, *Ocean waves and oscillating systems: linear interactions including wave-energy extraction*, Cambridge: Cambridge University Press, 2004.

29. R. W. Yeung, "Added mass and damping of a vertical cylinder in finite depth waters," *Applied Ocean Research*, vol. 3, no. 3, pp. 119-133, 1980.

30. A. Hulme, "The wave forces acting on a floating hemisphere undergoing forced periodic oscillations," *Journal of Fluid Mechanics*, vol. 121, pp. 443-463, 1982.

31. O. M. Faltinsen, S*ea loads on ships and offshore structures*, 1st ed. Cambridge: Cambridge University Press, 1993.